

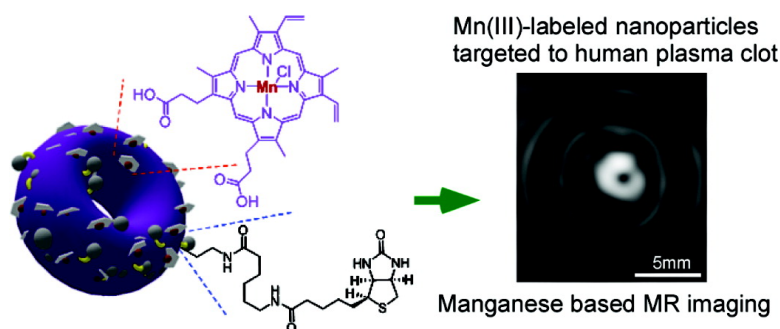
Communication

**Ligand-Directed Nanobialys as Theranostic Agent for Drug Delivery and Manganese-Based Magnetic Resonance Imaging of Vascular Targets**

Dipanjan Pan, Shelton D. Caruthers, Grace Hu, Angana Senpan, Mike J. Scott, Patrick J. Gaffney, Samuel A. Wickline, and Gregory M. Lanza

*J. Am. Chem. Soc.*, **2008**, 130 (29), 9186-9187 • DOI: 10.1021/ja801482d • Publication Date (Web): 24 June 2008

Downloaded from <http://pubs.acs.org> on February 8, 2009



**More About This Article**

Additional resources and features associated with this article are available within the HTML version:

- Supporting Information
- Access to high resolution figures
- Links to articles and content related to this article
- Copyright permission to reproduce figures and/or text from this article

[View the Full Text HTML](#)

## Ligand-Directed Nanobialys as Theranostic Agent for Drug Delivery and Manganese-Based Magnetic Resonance Imaging of Vascular Targets

Dipanjana Pan,<sup>\*,†</sup> Shelton D. Caruthers,<sup>†,‡</sup> Grace Hu,<sup>†</sup> Angana Senpan,<sup>†</sup> Mike J. Scott,<sup>†</sup> Patrick J. Gaffney,<sup>§</sup> Samuel A. Wickline,<sup>†</sup> and Gregory M. Lanza<sup>†</sup>

*C-TRAIN and Division of Cardiology, Washington University School of Medicine, 4320 Forest Park Avenue, Saint Louis, Missouri 63108, Philips HealthCare, Andover, Massachusetts, and Department of Surgery, St. Thomas's Hospital, London, U.K.*

Received February 29, 2008; E-mail: dipanjan@wustl.edu

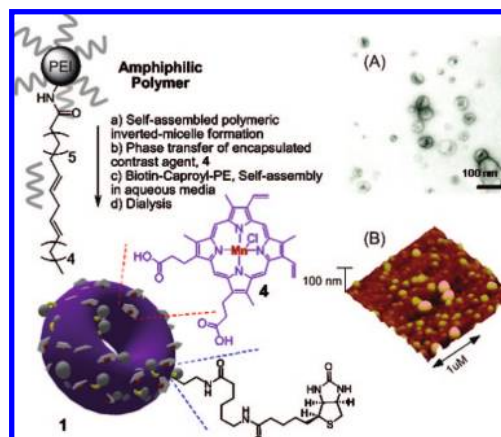
Noninvasive magnetic resonance (MR) molecular imaging and targeted drug delivery systems, often referred to as theranostic agents, are being developed to enable improved detection, patient risk stratification, site-specific treatment, and longitudinal monitoring.<sup>1</sup> One example of these agents, a gadolinium-based perfluorocarbon nanoparticle, has been used to detect, characterize, treat, and follow angiogenesis in preclinical models of cancer and atherosclerosis.<sup>11</sup>

Despite the preclinical success of this and related nanotechnology platforms, the recent discovery of nephrogenic systemic fibrosis (NSF), a serious and unexpected side effect of gadolinium blood pool agents observed in some patients with renal disease or following liver transplant, has cast a shadow on currently approved MR contrast agents.<sup>2</sup> Patients with NSF develop thickening of the skin and connective tissues that can inhibit arm and leg movements and even lead to bone fractures. Approximately 5% of patients experience a rapidly progressive course, which may result in death due to widespread fibrosis. The cause of NSF is unknown and there is no effective treatment of this condition. Although gadolinium has been the dominant paramagnetic metal for MR contrast agents, the issue of NSF has induced consideration of alternative approaches.

Manganese was one of the first reported examples<sup>3,4</sup> of paramagnetic contrast material studied in cardiac and hepatic MRI because of its efficient  $R_1$  enhancement. Similar to  $\text{Ca}^{2+}$  and unlike the lanthanides, manganese is a natural cellular constituent, and often a cofactor for enzymes and receptors. Manganese blood pool agents, such as mangafodipir trisodium, have been approved as a hepatocyte-specific contrast agent with transient side-effects due to dechelation of manganese from the linear chelate. Nontargeted liposomal agents have included  $\text{MnSO}_4$ <sup>3c</sup> or  $\text{Mn-DTPA}$ .<sup>3d</sup> Release of Mn caused by disruption of the vesicles allowed MR detection of sites where the vesicles were non-specifically entrapped.

Manganese(III)-labeled nanobialys (**1**) are a potential targeted MR theranostic nanoparticle produced by molecular self-assembly of amphiphilic branched polyethylenimine, which has a toroidal shape, tunable particle size, and low polydispersity. The "bialy" shape affords increased stability and presents kinetically stable, porphyrin coupled Mn(III) complexes directly to the surrounding water. In a typical synthesis, commercially available branched polyethylenimines (MW = 10 kDa) are hydrophobically modified (nominal 55% conjugation of the 1° amine) with linoleic acid by activating the carboxylic acid groups with 1-(3'-dimethylamino-propyl)-3-ethylcarbodiimide methiodide (1.2 equiv) and allowing the reaction overnight at ambient temperature. Supramolecular self-assembly of the amphiphilic polymer in anhydrous chloroform,

**Scheme 1.** Preparation of Nanobialys<sup>a</sup> and (A) TEM<sup>b</sup> and (B) AFM Image of Nanobialys



<sup>a</sup> Conditions: (a) Anhydrous chloroform, gentle vortexing, room temp; (b) aqueous solution of **4**, inversion, room temp, filter using short bed of sodium sulfate and cotton; (c) Biotin-Caproyl-PE, filter mixed organic solution using cotton bed, 0.2  $\mu\text{M}$  water, vortex, gently evaporation of chloroform at 45°C, 420 mbar, 0.2  $\mu\text{M}$  water, sonic bath, 50 °C, 1/2 h, dialysis (2 kDa MWCO cellulose membrane) against water. <sup>b</sup> Drop deposited over nickel grid, 1% uranyl acetate.

assumes inverted micellar<sup>5</sup> structures (**2**) that are able to transfer a water soluble new candidate contrast agent Mn(III)-protoporphyrin chloride (Mn-PPC, **4**) into chloroform. Synergistic self-assembly of the agent (**3**) alone or in presence of biotin-caproyl-DSPE (5 w/w% of total amphiphiles), presumably leads to the bilayer structure of nanobialys (**1**). The entrapment of manganese within the inverted micelles at the surface of the nanoparticles affords accessibility to water and eliminates detrimental interactions with surface homing ligands or surrounding plasma proteins. Nonbiotinylated (Mn(III)-labeled, **5**) and biotinylated nanobialys without metal (**6**) were produced as controls (Scheme 1).

Hydrodynamic particle size for the biotinylated without metal ( $180 \pm 9$  nm), biotinylated-Mn(III)-labeled ( $190 \pm 5$  nm) and nonbiotinylated-Mn(III) nanobialys ( $200 \pm 12$  nm) were similar with a narrow distribution (polydispersity  $0.18 \pm 0.01$ ,  $0.26 \pm 0.01$ , and  $0.17 \pm 0.01$ , respectively). In the anhydrous state, tapping mode atomic force microscopy (AFM) and transmission electron microscopy (TEM) revealed decreased particle height ( $H_{av} = 60 \pm 15$ ) and diameter ( $D_{av} = 95 \pm 26$ ) values. Characteristic changes in UV absorbance between 370 and 550 nm confirmed inclusion of the Mn(III)-porphyrin. Manganese content was  $25.6 \pm 03 \mu\text{g/mL}$  by ICP-OES, that is, 165 000 Mn(III) per nanobialy.

<sup>†</sup> Washington University School of Medicine.

<sup>‡</sup> Philips HealthCare.

<sup>§</sup> St Thomas's Hospital.

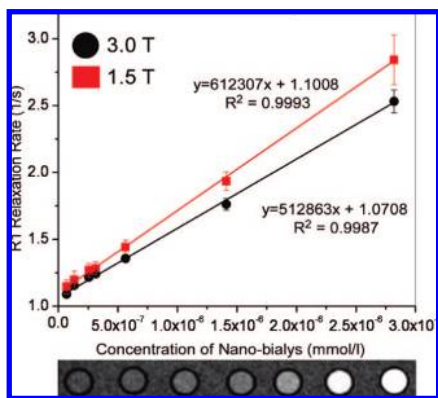


**Figure 1.** MRI results in suspension: longitudinal particulate  $r_1$  relaxivity. (Top) The measured  $r_1$  relaxation rate at 3.0 T (circles) and 1.5 T (squares) as a function of nanobialy concentration. (Bottom) A T1-weighted spin echo MR image (1.5 T) showing cross-sections of test tubes showing a bright signal from the high concentration (right) with progressively lower signal with dilution.

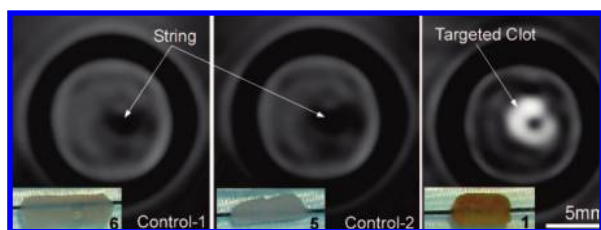


**Figure 2.** MRI images of fibrin-targeted nanobialys **1** (right) or control nanoparticles (**6** (left); **5** (middle)) bound to cylindrical plasma clots measured at 3.0 T. The ionic and particulate  $r_1$  relaxivities of serially diluted nanobialys at 3.0 T were  $3.1 \pm 1.1$  ( $\text{s} \cdot \text{mmol} [\text{Mn}]^{-1}$ ) and  $512\,863 \pm 8408$  ( $\text{s} \cdot \text{mmol} [\text{nanobialy}]^{-1}$ ), respectively.

A single slice inversion recovery sequence (i.e., the Look–Locker technique)<sup>6</sup> was used to calculate the ionic (per metal) and particulate (per particle)  $r_1$  relaxivities of serially diluted nanobialys at 1.5 T and 25 °C. The ionic  $r_1$  and  $r_2$  relaxivities of Mn(III)-labeled nanobialys were  $3.7 \pm 1.1$  ( $\text{s} \cdot \text{mmol} [\text{Mn}]^{-1}$ ) and  $5.2 \pm 1.1$  ( $\text{s} \cdot \text{mmol} [\text{Mn}]^{-1}$ ), respectively, and the particulate relaxivities were  $612\,307 \pm 7213$  ( $\text{s} \cdot \text{mmol} [\text{nanobialy}]^{-1}$ ) and  $866\,989 \pm 10704$  ( $\text{s} \cdot \text{mmol} [\text{nanobialy}]^{-1}$ ), respectively.

The concept of MR molecular imaging of fibrin, a critical component of intravascular thromboses, was studied in vitro. Fibrin-rich clots supported on silk suture were suspended in phosphate buffered saline (PBS, pH 7.4) with sealed polystyrene test tubes (75 mm). Nanobialys with biotin and metal (**1**), with biotin and no metal (**6**), or no biotin with metal (**5**) were targeted to the fibrin clots with classic avidin–biotin interactions and well-characterized biotinylated fibrin-specific monoclonal antibodies (NIB5F3).<sup>7</sup> Magnetic resonance images (3 T) of the clots were acquired using T1-weighted gradient echo images and a birdcage coil oriented with all groups visible within the imaging slice. MR images of clot samples (Figure 2) showed marked contrast enhancement of the fibrin-targeted Mn(III) nanobialys and no contrast improvement from the nontargeted and metal-free nanobialys.

The potential of nanobialys for drug delivery applications was assessed with two candidate chemotherapeutic agents, hydrophilic (e.g., doxorubicin) and hydrophobic (e.g., camptothecin) in vitro (see Supporting Information). Nanobialys were dialyzed in 60000 molecular weight cutoff dialysis tubing against an infinite sink of 0.9% NaCl, 0.2 mg/ml human serum albumin, and 0.05% sodium

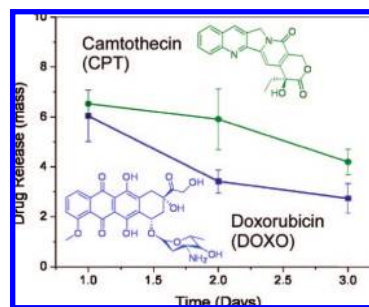


**Figure 3.** Dissolution assays: cumulative percent drug release in vitro from nanoparticles in dissolution over 3 days at 37 °C.

azide at 37 °C, which was sampled and replaced daily. The loading efficiencies of doxorubicin and camptothecin were  $98 \pm 0.1\%$  and  $99 \pm 0.1\%$ , respectively, by reverse phase HPLC. Drug release over 3 days was  $12 \pm 0.6\%$  for doxorubicin and  $20 \pm 3.5\%$  for camptothecin (Figure 3).

In summary, nanobialys are a novel theranostic agent, which offers the potential of site-specific MR T1-weighted molecular imaging with manganese (as opposed to gadolinium) as well as local delivery of potent chemotherapy agents. The utility of the MR targeted imaging is supported by its high particulate  $r_1$  relaxivity (at 1.5 and 3.0 T) and the strong MR contrast enhancement when targeted to clot. Incorporation of drugs with high efficiency and their retention in dissolution supports the theranostic potential of this platform technology.

**Acknowledgment.** The financial support from the NIH under the Grants NS059302, CA119342, and HL073646 and the NCI under the Grant N01CO37007 is greatly appreciated.

**Supporting Information Available:** Experimental details. This material is available free of charge via the Internet at <http://pubs.acs.org>.

## References

- (a) Winter, P. M.; Caruthers, S. D.; Wickline, S. A.; Lanza, G. M. *Nanofabrication towards Biomedical Applications* **2005**, 227–49. (b) Caruthers, S. D.; Wickline, S. A.; Lanza, G. M. *Curr. Opin. Biotechnol.* **2007**, *18*, 26–30. (c) Weissleder, R.; Kelly, K.; Sun, E. Y.; Shtatland, T.; Josephson, L. *Nat. Biotechnol.* **2005**, *23*, 1418. (d) Won, J.; Kim, M.; Yi, Y.-W.; Kim, Y. H.; Jung, N.; Kim, T. K. *Science* **2005**, *309*, 121. (e) Brown, M. A.; Semelka, R. C. *MRI: Basic Principles and Applications*, Wiley-Liss, New York, 2003. (f) Artemov, D. *J. Cellular Biochem.* **2003**, *90*, 518–24. (g) Hawker, C. J.; Wooley, K. L. *Science* **2005**, *309*, 1200–5. (h) O'Reilly, R. K.; Hawker, C. J.; Wooley, K. L. *Chem. Soc. Rev.* **2006**, *35*, 1068–83. (i) Whitesides, G. M. *Small* **2005**, *1*, 172–9. (j) Hummel, H.; Weiler, V. U.; Hoffmann, R. *PCT Int. Appl.* WO2006064451A2, 2006. (k) Unger, E. C.; Fritz, T. A.; Gertz, E. W. U.S. Pat. US6139819. (l) Nishiyama, N.; Kataoka, K. *Pharmacol. Ther.* **2006**, *11*, 630. (m) Wickline, S. A.; Lanza, G. M. *J. Cell. Biochem.* **2002**, (Suppl. 39), 90–7. (n) Winter, P. M.; Morawski, A. M.; Caruthers, S. D.; Fuhrhop, R. W.; Zhang, H.; Williams, T. A.; Allen, J. S.; Robertson, J. D.; Lanza, G. M.; Wickline, S. A. *Circulation* **2003**, *108*, 2270–4. (o) Turner, J. L.; Pan, D.; Plummer, R.; Chen, Z.; Whittaker, A. K.; Wooley, K. L. *Adv. Funct. Mater.* **2005**, *15*, 1248.
- (a) Kuo, P. H. *J. Am. Coll. Radiol.* **2008**, *5*, 29–35. (b) Abu-Alfa, A. K. *J. Am. Coll. Radiol.* **2008**, *5*, 45–52. (c) Ersoy, H.; Rybicki, F. J. *J. Magn. Reson. Imaging* **2007**, *26* (5), 1190–7.
- (a) Na, H. B.; Lee, J. H. *Angew. Chem., Int. Ed.* **2007**, *46*, 5397–401. (b) Caravan, P.; Ellison, J. J.; McMurry, T. J.; Lauffer, R. B. *Chem. Rev.* **1999**, *99*, 2293. (c) Ponce, A. M. *J. Natl. Cancer Inst.* **2007**, *99*, 53–63. (d) Schwendener, R. A. *Int. J. Pharm.* **1989**, *3*, 249–59.
- (a) Lauterbur, P. C.; Dias, M. H. M.; Rudin, A. M. In *Frontiers of Biological Energetics*, Dutton, P. L.; Leigh, J. S.; Scarpa, A., Eds.; Academic Press: New York, 1978, 752–9. (b) Mendonca-Dias, M. H.; Gaggelli, E.; Lauterbur, P. C. *Sem. Nucl. Med.* **1983**, *13*, 364–76. (c) Wendland, M. F. *NMR Biomed.* **2004**, *17*, 581–594.
- (a) Chechik, V.; Zhao, M.; Crooks, R. M. *J. Am. Chem. Soc.* **1999**, *121*, 4910–1. (b) Chen, Y. *Macromolecules* **2005**, *38*, 227–9.
- Look, D. C.; Locker, D. R. *Rev. Sci. Instrum.* **1970**, *41*, 621–7.
- Raut, S.; Gaffney, P. J. *Throm. Haemostasos* **1996**, *76*, 56–64.

JA801482D